Published in final edited form as:
Brain Res Bull. 2012 April 10; 87(6): 571–578. doi:10.1016/j.brainresbull.2012.01.012.

STRIATAL ATROPHY AND DENDRITIC ALTERATIONS IN A KNOCK-IN MOUSE MODEL OF HUNTINGTON'S DISEASE

Renata P. Lerner[*], **Luz del Carmen G. Trejo Martinez**[*], **Chunni Zhu**, **Marie-Françoise Chesselet**[‡], and **Miriam A. Hickey**
Department of Neurology, RNRC B114, 710 Westwood Plaza, UCLA David Geffen School of Medicine, Los Angeles, CA 90095 USA

Abstract

Huntington's disease (HD) is a progressive neurodegenerative disease characterized by progressive atrophy of the striatum, cerebral cortex, and white matter tracks. Major pathological hallmarks of HD include neuronal loss, primarily in the striatum, and dendritic anomalies in surviving striatal neurons. Although many mouse models of HD have been generated, their success at reproducing all pathological features of the disease is not fully known. Previously, we demonstrated extensive striatal neuronal loss and striatal atrophy at 20–26 months of age in a knock-in (KI) mouse model of HD. To further investigate this model, which carries a human exon 1 with ~119 CAG repeats inserted into the mouse gene (initially 140 repeats), we have examined whether these mice exhibit the atrophy and neuronal anomalies characteristic of HD. Stereological analyses revealed no changes in the striatal volume of male and female homozygote mice at 4 months, however striatal atrophy was already present at 12 months in both sexes. Analysis of cortical and corpus callosum volume in male homozygotes revealed a loss in corpus callosum volume by 20–26 months. At this later age, the surviving striatal neurons displayed extensive loss of spines in distal branch orders that affected both immature and mature spines. Mirroring late stage HD striatal neuronal morphology, the striatal neurons at this late age also showed reduced dendritic complexity, as revealed by Sholl analysis. Tyrosine hydroxylase immunoreactivity was also decreased in the striatum of 20–26 month old KI mice, suggesting an alteration in striatal inputs. These data further indicate that CAG140 homozygote KI mice exhibit HD-like pathological features and are a useful model to test the effects of early and/or sustained administration of novel neuroprotective treatments.

Keywords

Golgi stain; stereology; volume; huntingtin; cortex; corpus callosum

[‡]Author for correspondence and for reprint requests: Marie-Françoise Chesselet MD PhD, RNRC B114, Dept. Neurology, 710 Westwood Plaza, UCLA David Geffen School of Medicine, Los Angeles, CA, 90095, Tel: 310 267 1781, Fax: 310 267 1786, MChesselet@mednet.ucla.edu.
[*]These authors contributed equally to this work.

Conflict of interest statement: The authors declare that they have no conflict of interest.

1.0 INTRODUCTION

Huntington's disease (HD) is a progressive, autosomal dominant, neurodegenerative disorder that leads to deterioration of movement, mood and cognitive function. The disease is caused by an unstable elongated trinucleotide repeat in the *huntingtin* gene which results in the expression of mutant huntingtin protein with an extended stretch of glutamines in its N-terminal [19]. Mice expressing the HD-causing mutation are an invaluable tool for understanding the pathophysiology of the disorder and for testing therapies that could halt the course of HD, or prevent its onset in gene carriers. A critical question regarding the use of mouse models is how well they reproduce key pathological features of the disorder. Although many models exhibit functional disturbances, premature death, and characteristic aggregates of mutant huntingtin; only a few progress towards a loss of neurons in the striatum, thus failing to reproduce this cardinal sign of HD. Such deficit would be important for evaluating the neuroprotective effects of new therapeutics for HD.

Mice with the mutation "knocked-in" to the mouse HD gene (KI mice) have the advantage of expressing the mutation in the proper genomic and protein context of full-length huntingtin. Mice of this line originally carried human exon 1 with approximately 140 CAG repeats inserted in the mouse gene and were characterized for behavioral deficits and neuropathology over time [32]. Further studies of mice from the same line with approximately 120CAG repeats confirmed that these mice exhibit behavioral anomalies as early as 1 month of age and huntingtin pathology, including diffuse huntingtin nuclear staining, punctate nuclear and neuropil aggregates, and nuclear inclusions at 4 months [15, 32]. Cellular dysfunction, indicated by reduced expression of striatal mRNAs encoding enkephalin, DARPP-32, D1, D2, and CB1 is observed at 4 months of age, with reduced DARPP-32 immunohistochemistry by 12 months [14, 15]. The mice progress toward overt behavioral deficits at 24 months of age, at which time there is a 38% decrease in striatal volume and a 40% loss of striatal neurons [15]. The progressive time course of deficits in this model suggests that it is highly suited to testing drug interventions that could be beneficial at different stages of the disease. Little is known, however, of the time course of brain atrophy and whether the mice reproduce any of the characteristic features of neuronal pathology observed in post-mortem brains of patients with HD.

In the present study we sought to further investigate the use of the CAG140 KI mice as a model of HD pathology by measuring striatal, corpus callosum and cortical volumes in 4, 12, and 20–26 month old homozygote mutants and their wild-type (WT) littermates. In addition, we carried out quantitative analysis of the neuronal processes of surviving Golgi-stained striatal neurons of 20–26 month old mice. Finally, a tyrosine hydroxylase (TH) immunohistological stain was conducted in striatum from the 20–26 month old mice to determine whether the morphological anomalies were associated with loss of dopaminergic terminals in the striatum.

2.0 MATERIALS AND METHODS

2.1 Animals

All procedures were carried out in accordance with the NIH Guide for the Care and Use of Laboratory Animals (NIH Publications No. 80-23) revised 1996, and were approved by the Institutional Animal Care and Use Committee at UCLA. All analyses were carried out by blinded observers/scorers. Mice used in this study were on a mixed C57BL/6J × 129/Sv background (N3 on C57BL/6J). All KI mice used in this study were homozygous for the mutation. Mice were generated from heterozygote breeding pairs (only non-sibling breeding pairs were used). The repeat lengths from a sample of the KI mice used in this study were 119 ± 3.2 (mean ± sem, n = 8, Laragen Inc., Culver City, CA, USA). We have examined

CAG140 KI mice extensively for both behavior and pathology using mice with a very similar repeat length (~121, [15]) to the mice used in the current study (~119). Body weight was unaffected by genotype in mice carrying ~121 repeats [36] or repeat length of approximately 140 [32] at less than 1 year of age. Food and water were available *ad lib* and mice were kept on a reverse 12-h light/dark cycle.

2.2 Volume measurements

Male mice were used for stereological volume measurements of the striatum, corpus callosum and cortex (4 months, n=4–5; 12 months, n=3–4; 20–26 months, n=4–7) and female mice were used for additional volume measurements of striatum (4 months n=3; 12 months n=3). Mice were perfused with 4% paraformaldehyde and brains were then dissected out. The hemispheres were separated and postfixed overnight and then cryoprotected in 30% sucrose and frozen for analysis except that for a subset of 20–26 month old mice one hemisphere was not frozen and was instead processed for Golgi staining. Coronal cryosections from the frozen hemispheres were cut (35 μm) and stored in cryoprotectant until processing. The volume of striatum was measured in sections from bregma +1.94 through −0.46 [35] i.e. from the front of the striatum to levels slightly posterior to the level of the crossing of the anterior commissure, similar to previous analyses in HD mice [6, 25, 44]. In two previous analyses, we found that striatal volume at this level correlated to total volume with r^2= 0.98 or r^2= 0.73 ($p<0.0001$, data not shown, n=11; $p<0.0001$, data not shown, n=14; respectively), indicating that it is representative of total striatal volume. Furthermore, this volume represents 82–86% of total striatal volume. The volume of the cortex and corpus callosum was determined from the sections used for striatal measurements. For stereological analyses, the first section of the stereological series was chosen at random from the first 10 sections of the region of interest, to eliminate bias. Every 10^{th} section thereafter was chosen such that 350 μm was the advance between each section. Sections were stained with cresyl violet, according to manufacturer's instructions (Fisher Scientific, Pittsburgh, PA). The striatum, corpus callosum and cortex were outlined in each section using StereoInvestigator V5.00 (MicroBrightField Inc., Colchester, VT), at 5× using a 1.4 NA lens and 1.4 NA oil condenser, with a DVC realtime digital camera (Digital Video Camera Company, Austin, TX). The boundaries used for striatum included the corpus callosum and followed the external capsule as ventrally as possible. The line then continued across to the most ventral point of the lateral ventricle (excluding the anterior commissure) and continued along the lateral ventricle until it reached the corpus callosum again. Overlying cortex (excluding the piriform cortex) was used for cortical measurements. The program calculated the outlined area. Volumes were calculated using the Cavalieri method. All measurements were conducted by an observer blinded to the mouse genotype.

2.3 Golgi Staining

One hemisphere from a subset of 20–26 month old mice used for stereology (WT, n=3; KI, n=4) was cut into 100 μm sagittal sections and stained as per manufacturer guidelines (FD Neurotechnology, MD) by the UCLA Microscopic Techniques Core. The striatum was identified and defined at 4X magnification. For gross morphology, medium sized spiny neurons in the dorsal region of the striatum were drawn at 40X magnification using a CHS Olympus Hi Tech Instruments, Inc. microscope and a camera lucida. Spine morphology was drawn and examined at 100X magnification.

We identified 10 Golgi-stained neurons from each mouse using the following criteria 1) at least three dendrites per soma and 2) one dendrite from each neuron with at least a second order branch. The drawings were then scanned into digital format using an Epson, Stylus RX580 scanner for NIH ImageJ analysis. ImageJ was used to determine soma size, dendritic length and dendritic diameter. The dendritic diameter for each neuron was calculated from

the mean of three measurements per branch. Dendritic fields were measured using Sholl analysis (ImageJ). The number of primary dendrites, spine density, and spine morphology were measured at the time of drawing. The dendrite with the greatest number of branch orders (for each neuron) was used for spine density and spine morphology measurements. The immature and mature spines were identified using a qualitative scale [22, 39]. Briefly, spines were grouped into immature or mature groups depending on spine neck thickness and length, in addition to bouton morphology, as previously described [22, 39]. Distal dendrites were also analyzed for the presence or absence of wavy extensions, as a measurement of dysmorphic neurons, as previously described [28]. All measurements were conducted by an observer blinded to the mouse genotype.

2.4 Tyrosine hydroxylase staining

Immunohistochemical staining for TH was performed on free-floating cryosections from the frozen hemisphere of a subset of the 20–26 months old mice that were used for stereology with one additional KI mouse (WT n=6, KI n=5). Sections were washed in 0.1 M phosphate-buffered saline (PBS, 3 × 10 mins) and then incubated in 10% NGS normal goat serum, in 0.5% Triton/PBS for 1 h. Sections were then incubated in rabbit anti-TH (1:500) antibody in 0.5% Triton X, 5% NGS and PBS at 4°C overnight (Millipore, Temecula, CA). Control sections were incubated in 5% NGS/PBS at 4°C overnight. The following day, unbound primary antibody was washed off with 0.1 M PBS (3×10 min washes). Sections were incubated in Cy3-conjugated goat anti-rabbit antibody (1:500) diluted in 5% NGS for 1 h, followed by washes in 0.1 M PBS (3 × 10 min). Sections were then mounted onto gelatin-coated slides and scanned with an Agilent DNA microarray scanner (Agilent Technologies Inc., Santa Clara, CA) at 10 μm resolution. Fluorescence intensity of cortical regions with no detectable immunostained terminals (background) and of striatum were determined for each section using ImageJ, and the relative fluorescence intensity calculated by subtracting the background from striatal fluorescence intensity. No specific staining was observed in control sections (no primary antibody). All measurements were conducted by an observer blinded to the mouse genotype.

2.5 Statistics

All statistical analyses were performed using raw data and are represented as mean ± sem. Volume data were expressed as a percent of WT values for graphic purpose only. Striatal volume of male and female mice was analyzed using a completely randomized three-way ANOVA with genotype, gender and age (4 and 12 months) as factors, followed by Fisher's LSD post hoc tests. Cortical and corpus callosal volumes were also analyzed with separate completely randomized two-way ANOVAs with genotype and age (4, 12 and 20–26 months) as factors, followed by Fisher's LSD post hoc tests. We also analyzed cortical, striatal and corpus callosum volume at 4 and 12 months using two-way repeated measures ANOVAs, where anatomical area (cortex, striatum and corpus callosum) was used as the repeating factor and genotype was used as the additional factor, followed by Fisher's LSD post hoc tests. Power calculations used striatal data from male CAG140 KI mice, using WT striatal volume as the target volume. For Golgi staining, the mean for each mouse was used to generate group means. Frequency distribution, Sholl analysis and spine densities were analyzed by repeated measures ANOVAs (with genotype, and soma size, distance from soma, or branch order, respectively as factors) followed by Fisher LSD post hoc tests. Mean soma size, mean dendritic length and mean TH fluorescence were compared with two-tailed Student's t tests. GBStat (V8.0) was used for all statistics. A critical value of $p<0.05$ was used for all comparisons.

3.0 RESULTS

3.1 Striatal, cortical, and corpus callosum volume estimates

We have previously reported that striatal volume is decreased by 38% in the brain of ~24 month old male CAG140 KI mice compared with WT littermates [15]. In the present study, we extend these data by examining striatal volume in both male and female mice at younger ages, and the volume of the overlying corpus callosum and cortex in male mice across time. Measurements of striatal volume were conducted from the rostral part of the striatum to a level caudal to the anterior commissure crossing (from bregma +1.94 through −0.46; 35). In previous analyses we found that striatal volume at this level correlated to total volume with r^2= 0.98 or 0.73 ($p<0.0001$, n=11 and $p<0.0001$, n=14, respectively), indicating that it is representative of total striatal volume. Striatal volume was measured in both male and female mice at 4 and 12 months of age and analyzed by randomized 3 way ANOVA: effect of genotype $F(1,20)=15.7$, $p<0.001$; genotype × gender interaction $F(1,20)=0.4$, ns; genotype × age $F(1,20)=4.4$, $p<0.05$; genotype × gender × age $F(1,20)=0.1$, ns; 4 month males: WT: 6.4 ± 0.3 mm^3; KI: 5.8 ± 0.4 mm^3; Fisher's LSD, ns (Fig. 1A); 4 month females: WT: 6.5 ± 0.8 mm^3; KI: 6.0 ± 0.5 mm^3; Fisher's LSD, ns; 12 month males: WT: 8.0 ± 0.5 mm^3; KI: 5.8 ± 0.4 mm^3; Fisher's LSD, $p<0.01$ (Fig. 1A); females: WT: 6.4 ± 0.2 mm^3; KI: 4.9 ± 0.2 mm^3; Fisher's LSD, $p<0.05$. Thus, no deficit in striatal volume was present at 4 months of age in either male or female KI mice. However, we observed a significant striatal atrophy by 12 months of age in both male (−27%) and female (−24%) homozygous KI mice. At this age, n=3 male mice are sufficient to detect normalization of striatal volume to the level of male WT mice based on power calculations using $\alpha = 0.05$ and 90% power.

To determine whether atrophy of extrastriatal regions also occurred in these mice, we measured the volume of the corpus callosum and of the cerebral cortex directly overlying the striatum, at the level used for the analysis of striatal volume, in male homozygous mice. The cortex and corpus callosum were analyzed separately using genotype and age (4, 12 and 20–26 months) as variables. No significant change in cortical volume was detected by ANOVA: effect of genotype $F(1,21)=4.0$, ns; effect of age, $F(2,21)=2.2$, ns.; genotype × age interaction, $F(2,21)=0.8$, ns.: at 4 months of age WT: 11.6 ± 0.9 mm^3; KI: 10.8 ± 0.9 mm^3; 12 months of age: WT: 13.2 ± 0.8 mm^3; KI: 11.9 ± 1.3 mm^3; 20–26 months: WT, 15.6 ± 1.0 mm^3; KI, 11.9 ± 1.6 mm^3 (Fig 1B).

In contrast, for the corpus callosum, ANOVA indicated no effect of genotype ($F(1,21)=2.6$, ns) or genotype × age interaction ($F(2,21)=2.0$, ns) but an effect of age ($F(2,21)=3.5$, $p<0.05$; 4 months: WT: 1.9 ± 0.1 mm^3; KI: 2.0 ± 0.2 mm^3; Fisher's LSD, ns; 12 month: WT: 2.0 ± 0.2 mm^3; KI: 1.8 ± 0.2 mm^3; Fisher's LSD, ns; 20–26 months: WT: 3.1 ± 0.3 mm^3; KI: 2.1 ± 0.2 mm^3; Fisher LSD $p<0.05$), indicating a volume reduction (−33%) by 20–26 months in CAG140 male KI mice (Fig. 1B).

Together, these data indicate that CAG140 KI mice show robust atrophy in brain, with an initial loss in striatal volume, compared to WT mice, at 12 months, and a later reduction in corpus callosum volume at 20–26 months. Nonetheless this atrophy occurs many months after initial behavioral deficits are found [15]. This suggests that striatal volume measurements at 12 month of age would provide a useful measure for preclinical drug trials, whereas time-consuming measurements of corpus callosum would only be informative at much older ages.

3.2 Golgi staining

We analyzed Golgi-stained medium sized spiny neurons in striatum from CAG140 WT and KI mice at 20–26 months of age (representative neuron, Fig. 2). Mean soma size and the

relative frequency distributions of soma sizes were similar between WT and homozygote mutant (KI) mice (Fig. 2, frequency distribution, genotype × soma size interaction $F(7,35)=0.76$, ns; mean size, WT, 129.8 ± 3.5μm^2, KI, 127.3 ± 4.7μm^2, Student's t test, ns). Total branch length and dendritic diameter were also similar between WT and KI mice; however, there was a trend towards reduced dendritic total length in KI mice (Fig. 3, left, dendritic diameter: effect of genotype $F(1,5)=0.2$, ns; effect of branch order $F(4,20)=67.1$, $p<0.0001$; genotype × branch order $F(4,20)=0.8$, ns; right, total branch length: 11% reduction, Student's t test, ns). Indeed, analysis of dendritic complexity using Sholl analysis revealed reduced intersections at 40–60μm from the soma, when compared to WT mice (Fig. 4, effect of genotype $F(1,5)=9.8$, $p<0.03$; effect of distance $F(9,45)=125.0$, $p<0.0001$; genotype × distance from soma, $F(9,45)=0.6$, ns; WT versus KI at 40 and 50 μm, Fisher's LSD, $p<0.05$; WT versus KI at 60 μm, Fisher's LSD, $p<0.01$). Results are indicative of reduced dendritic arborization and complexity, similar to observations in medium sized spiny neurons of the striatum in late stage HD and in transgenic R6/2 mice [9, 27]. We also examined whether dendrites were wavy [i.e., dysmorphic, [28]], but in mice of this age (20–26 months) we did not detect any differences between WTs and KIs (data not shown).

With regard to spine density and spine morphology, we found that proximal branch orders (1–2) contained few spines, but with increasing distance from the soma, the density of spines increased, as is well-known (Fig. 5, effect of branch order, $F(4,20)=59.2$, $p<0.0001$). Despite the advanced age of the mice, spine density in WT mice was comparable to previously published data in younger normal mice [27]. In KI mice, a large decrease in spine density was found in the 3rd, 4th and 5th branch orders (Fig. 5, effect of genotype $F(1,5)=9.1$, $p<0.03$; genotype × branch order $F(4,20)=1.8$, ns; branch order 3, WT versus KI, Fisher's LSD, $p<0.05$; branch orders 4 and 5, WT versus KI, Fisher's LSD, $p<0.01$). These results are reminiscent of observations made in medium sized spiny striatal neurons from severe grade IV HD brains [9, 10].

We then analyzed whether immature and mature spines were affected equally. Spines were identified as mature or immature based on previously published qualitative criteria, involving length and thickness of neck, in addition to bouton morphology [22, 39]. Both immature and mature spines were reduced in KI mice (Fig. 6, immature spines: effect of branch order $F(4,20)=13.9$, $p<0.0001$; genotype × branch order $F(4,20)=1.9$, ns; branch orders 4 and 5, WT versus KI, Fisher's LSD, $p<0.05$; mature spines: effect of branch order $F(4,20)=28.8$, $p<0.0001$, genotype × branch order $F(4,20)=1.4$, ns; branch order 5, WT versus KI, Fisher's LSD, $p<0.05$). However, immature spines were more affected in KI mice than mature spines with a greater loss of immature spines in distal branches (KI mice: branches 3 through 5: 28–47% loss of immature spines; 12–38% loss of mature spines; immature versus mature spines: overall effect of genotype $F(1,10)=9.2$, $p<0.02$; overall effect of maturity, $F(1,10)=8.4$, $p<0.02$; overall effect of branch order $F(4,40)=46.1$, $p<0.0001$; genotype × maturity × branch order $F(4,40)=0.3$, ns; KI, immature versus mature, branch orders 3 and 4, Fisher's LSD, $p<0.05$ and $p<0.01$, respectively; WT, no significant difference in density of immature versus mature spines at any branch order).

Both glutamatergic and dopaminergic inputs contribute to spine morphology [33]. Specifically, dopamine deficiency has been associated with a loss in spines in medium sized spiny neurons [4, 20, 21, 33, 46], and dopamine is being increasingly considered as a potential neuroprotective agent in HD [16, 29, 49]. Therefore, to determine whether alterations in DA transmissions could contribute to the morphological impairments we have observed in older mice, we performed an immunocytochemical stain for TH, a marker of nigrostriatal dopaminergic terminals in the striatum. 20–26 month old KI mice showed a significant loss of striatal TH immunoreactivity (Fig. 7, Student's t test, $p<0.002$).

4.0 DISCUSSION

HD is a progressive disorder and new evidence indicates that the onset of the characteristic neurological symptoms is preceded by a protracted premanifest phase of disease [34, 47, 48]. Because carriers can be readily identified with genetic testing, early implementation of neuroprotective treatments will eventually be possible once such treatments are identified. At this time, however, no cure or methods to delay or prevent the onset of the devastating symptoms of HD are available, and the development of such treatments is predicated on preclinical testing in mouse models of the disease. Of the many models available, the CAG140 mice present many advantages both because they express a full length mutated protein and because they express robust behavioral deficits that are suitable for drug testing, from an early age. Previous characterization of the pathological features of this model has been limited to a description of huntingtin pathology [32] and the discovery of late stage striatal atrophy and neuronal loss [15].

In the present study, we show that this striatal atrophy develops over time as with HD. We observed no deficit in striatal volume at 4 months of age but by 12 months there was decreased volume in both male and female homozygote KI mice. In addition, we show that atrophy of the corpus callosum is present at 20–26 months of age and that surviving neurons in the striatum show significant morphological alterations at that age. These data further establish the validity of this mouse model for studies of neurodegeneration and its prevention, and provide time course information on some of the major endpoint measures and robust differences that can be used in preclinical drug testing of neuroprotective therapies for HD.

It is noteworthy that the decrease in striatal volume we have observed in CAG140 mice (repeat length of ~119 CAGs in this study) does not occur until many months after the onset of behavioral deficits that have been detected as early as 1 month of age in this model. Carriers of the HD mutation also show subtle behavioral deficits many years before the onset of clear neurological symptoms [34, 45, 47, 48]. Similarly, CAG94 KI mice show ~14% loss in striatal volume, but no loss in neuronal number, at approximately 2 years of age whereas behavioral deficits begin at 2 months [32]. Nevertheless, as in HD [34, 48], striatal atrophy was detected in our model many months before the onset of overt behavioral deficits (approximately 20–26 months of age [15]). Notably, the striatal atrophy detected at this late age is similar to the “one third to one half loss” demonstrated in HD patients at the time of diagnosis [2].

Alterations in white matter tracts have been described to occur very early in carriers of the HD mutation [48]. Neither the volumes of the cerebral cortex nor the corpus callosum, measured in the same sections as the striatum, were altered at 12 months, when striatal atrophy was already evident. This result in cortex however, should be interpreted with caution because it reflects only a small portion, and a global measure of cortex can miss specific atrophy of defined cortical layers, as has been observed in patient brain [40, 42]. Similarly, our corpus callosum measurements were global, which could obscure subtle changes, as have been found in HD [3]. Nevertheless, a significant decrease in the volume of the corpus callosum was detected at 20–26 months of age, confirming that white matter tracts are affected in this model, as they are at early stages of HD [41, 43].

The existence of morphological anomalies of surviving striatal neurons in post-mortem tissue from HD patients has been well documented but these studies are usually performed at relatively advanced stages of disease [9, 10]. We found that at a time when about 40% of striatal neurons are lost and overt behavioral deficits just become apparent, remaining striatal neurons in our mouse model present significant morphological alterations suggesting

the presence of a slow, ongoing neurodegenerative process. Specifically, the neurons showed a significant reduction in spine density, preferentially lost in the distal branches of the dendrite, as well as a reduced dendritic arborization, and a trend toward a reduction in total dendritic branch length. Thus, the CAG140 KI mice offers an opportunity to analyze the mechanisms that lead to cellular pathology characteristic of HD, in addition to allowing the testing of potential neuroprotective agents.

It is clear that both intrinsic and extrinsic mechanisms contribute to the demise of striatal neurons in HD [11–13, 18, 50]. A role for cortical inputs has been documented in mouse models [12, 13], however another intriguing possibility is the potential role of dysfunction in the other main striatal input, the dopaminergic neurons from the Substantia nigra pars compacta that are more commonly thought of as the primary deficit in Parkinson's disease. In humans, a reduction in dopamine receptors has been demonstrated in both symptomatic and asymptomatic HD patients [1, 37, 38, 51]. Early loss of dopamine receptors, abnormal transcriptional levels of dopamine-regulated proteins, reduced dopamine release, reduced dopamine levels, have all been observed in the striatum of HD mice [5, 14, 16, 23, 49]. In CAG 140 KI mice, we have shown reduction in D1 and D2 dopamine receptor mRNAs as early as 4 months of age [14, 17]. On the presynaptic side, some studies have detected a loss of striatal dopamine in post-mortem brains of HD patients [26] although the data have been inconsistent [30, 31]. In the present study, we have measured immunoreactivity of TH, the rate-limiting enzyme of catecholamine synthesis and a marker for dopamine terminals in the striatum (which contains very few noradrenergic terminals). Interestingly, several studies have reported an association between striatal dopamine deficiency and spine loss in medium sized spiny neurons [4, 20, 21, 33, 46]. In fact, changes in dopamine function influencing striatal spines in HD could either be pre- or post-synaptic. Importantly, our measurements here were made using a fluorescently-labeled secondary antibody and measured with a microarray scanner. This method provides enhanced correlation of signal intensity to antigen concentration because, contrary to diaminobenzidine based immunodetection techniques, it does not rely on an enzymatic reaction and it uses the expanded dynamic range of fluorescence. TH immunofluorescence was markedly reduced, and although no non-perfused tissue from these very old mice was available to perform neurochemical studies, previous data in R6/2 mice, a severe model of HD, suggests that striatal dopamine is reduced in old mutant mice [16].

It is tempting to interpret these data to suggest that dopamine therapy could be beneficial in HD. Unfortunately, although L-dopa administration was found to improve short-term symptoms in R6/2 mouse models, its long-term administration was deleterious to behavior and survival [16]. Moreover, high-dose L-dopa treatment has not been shown to restore spine density back to normal levels in either PD models or patients, demonstrating that an increase in dopamine does not recover the pathology [8]. Perhaps dopamine needs to be administered earlier, or other factors present in dopaminergic or other terminals contribute to the morphological deficits in striatal neurons.

Indeed, another factor that could lead to spine loss is excess glutamate. Studies in mouse models of HD have revealed increases in corticostriatal glutamate currents that occur early in the course of the disease [24, 28]. In our study, we found that distal branches of the dendrites suffered greater spine loss than those of the proximal dendritic branches. As the distal dendrites are associated with growth and with relatively greater spine densities, they are more susceptible to excessive activity of glutamatergic inputs and the resulting increase in calcium levels that could lead to their degeneration [9]. At later disease stage, some mouse models exhibit a disconnection of the corticostriatal synapse [7, 24]. Although it is not known whether a cortical disconnection results in spine degeneration, or whether the

spine degeneration is itself the cause of the cortical disconnection, it is clear that at the late stage examined in our study, neuronal function is severely compromised.

In conclusion, we report loss in striatal volume from 12 months of age in both male and female mice, with loss in corpus callosum volume by 20–26 months, and show that surviving neurons in the striatum of 20–26 month old mice exhibit degenerative changes in morphology, in particular loss of both immature and mature spines in distal branches. This was accompanied by a decrease in striatal TH immunohistochemical staining, suggesting a loss of dopaminergic input to the striatum at this age. Together, these data reveal additional endpoint measures for neuroprotective studies. Our data clearly indicate that therapies should target earlier stages of pathophysiology, prior to the occurrence of irreversible cellular impairments that occur during disease progression. This is because the striatal atrophy, and the morphological anomalies, present in striatal neurons in our mouse model at 20–26 months are likely to correspond to early manifest HD. The CAG140 KI mice provides a useful model to analyze the effects of potential neuroprotective treatments on both short- and long-term effects of the HD mutation, correlating to different stages of disease. Furthermore, the protracted period of time between the appearance of subtle but robust behavioral deficits at 1 month of age and evidence of frank neurodegeneration allows for the testing of early and sustained neuroprotective interventions in this model, and provides a long therapeutic time window in this model of HD, as occurs in HD itself.

Highlights

- Here, we show striatal atrophy is already present at 12 months in CAG140 KI mice
- We also show late-disease-stage (20–26m) atrophy in white matter in CAG140 KI mice
- Late-disease-stage KI striatal neurons display extensive morphological degeneration
- DA input may be altered in late-disease-stage KI striatum, as striatal TH is reduced
- CAG140 KI mice are highly suited for testing neuroprotective therapies

Acknowledgments

We wish to thank Marianne Cillufo of the UCLA Microscopic Techniques Core for the Golgi staining. We also thank Dr Michael Levine, Director of the HD mouse colony, for his support, and Gowry Fernando, Zhongliang Zhang and Janelle Asai for expert assistance with the mouse colony.

Support: CHDI, Inc. and private funds to MFC

BIBLIOGRAPHY

1. Antonini A, Leenders KL, Spiegel R, Meier D, Vontobel P, Weigell-Weber M, Sanchez-Pernaute R, de Yébenez JG, Boesiger P, Weindl A, Maguire RP. Striatal glucose metabolism and dopamine D_2 receptor binding in asymptomatic gene carriers and patients with Huntington's disease. Brain. 1996; 119:2085–2095. [PubMed: 9010012]
2. Aylward EH. Change in MRI striatal volumes as a biomarker in preclinical Huntington's disease. Brain Res. Bull. 2007; 72:152–158. [PubMed: 17352939]
3. Aylward EH, Nopoulos PC, Ross CA, Langbehn DR, Pierson RK, Mills JA, Johnson HJ, Magnotta VA, Juhl AR, Paulsen JS. Longitudinal change in regional brain volumes in prodromal Huntington disease. J Neurol Neurosurg Psychiatry. 2011; 82:405–410. [PubMed: 20884680]
4. Azdad K, Chavez M, Don Bischop P, Wetzelaer P, Marescau B, De Deyn PP, Gall D, Schiffmann SN. Homeostatic plasticity of striatal neurons intrinsic excitability following dopamine depletion. PLoS One. 2009; 4:e6908. [PubMed: 19730738]

5. Bibb JA, Yan Z, Svenningsson P, Snyder GL, Pieribone VA, Horiuchi A, Nairn AC, Messer A, Greengard P. Severe deficiencies in dopamine signalling in presymptomatic Huntington's disease mice. Proc. Natl. Acad. Sci. USA. 2000; 97:6809–6814. [PubMed: 10829080]
6. Chopra V, Fox JH, Lieberman G, Dorsey K, Matson W, Waldmeier P, Housman DE, Kazantsev A, Young AB, Hersch S. A small-molecule therapeutic lead for Huntington's disease: preclinical pharmacology and efficacy of C2–8 in the R6/2 transgenic mouse. Proc. Natl. Acad. Sci. USA. 2007; 104:16685–16689. [PubMed: 17925440]
7. Cummings DM, Cepeda C, Levine MS. Alterations in striatal synaptic transmission are consistent across genetic mouse models of Huntington's disease. ASN Neuro. 2010; 2:e00036. [PubMed: 20585470]
8. Deutch AY, Colbran RJ, Winder DJ. Striatal plasticity and medium spiny neuron dendritic remodeling in parkinsonism. Parkinsonism Relat. Disord. 2007; 13 Suppl 3:S251–S258. [PubMed: 18267246]
9. Ferrante RJ, Kowall NW, Richardson EP Jr. Proliferative and degenerative changes in striatal spiny neurons in Huntington's disease: a combined study using the section-Golgi method and calbindin D28k immunocytochemistry. J. Neurosci. 1991; 11:3877–3887. [PubMed: 1836019]
10. Graveland GA, Williams RS, DiFiglia M. Evidence for degenerative and regenerative changes in neostriatal spiny neurons in Huntington's disease. Science. 1985; 227:770–773. [PubMed: 3155875]
11. Gray M, Shirasaki DI, Cepeda C, Andre VM, Wilburn B, Lu XH, Tao J, Yamazaki I, Li SH, Sun YE, Li XJ, Levine MS, Yang XW. Full-length human mutant huntingtin with a stable polyglutamine repeat can elicit progressive and selective neuropathogenesis in BACHD mice. J. Neurosci. 2008; 28:6182–6195. [PubMed: 18550760]
12. Gu X, Andre VM, Cepeda C, Li SH, Li XJ, Levine MS, Yang XW. Pathological cell-cell interactions are necessary for striatal pathogenesis in a conditional mouse model of Huntington's disease. Mol. Neurodegener. 2007; 2:8. [PubMed: 17470275]
13. Gu X, Li C, Wei W, Lo V, Gong S, Li SH, Iwasato T, Itohara S, Li XJ, Mody I, Heintz N, Yang XW. Pathological cell-cell interactions elicited by a neuropathogenic form of mutant Huntingtin contribute to cortical pathogenesis in HD mice. Neuron. 2005; 46:433–444. [PubMed: 15882643]
14. Hickey, MA.; Franich, NR.; Medvedeva, V.; Chesselet, MF. Mouse models of mental illness and neurological disease: Huntington's disease. In: Watson, C.; Paxinos, G.; Puelles, L., editors. The Mouse Nervous System. London: Elsevier; in press.
15. Hickey MA, Kosmalska A, Enayati J, Cohen R, Zeitlin S, Levine MS, Chesselet MF. Extensive early motor and non-motor behavioral deficits are followed by striatal neuronal loss in knock-in Huntington's disease mice. Neuroscience. 2008; 157:280–295. [PubMed: 18805465]
16. Hickey MA, Reynolds GP, Morton AJ. The role of dopamine in motor symptoms in the R6/2 transgenic mouse model of Huntington's disease. J. Neurochem. 2002; 81:46–59. [PubMed: 12067237]
17. Hickey MA, Zhu C, Medvedeva V, Franich NR, Levine MS, Chesselet M-F. Evidence for behavioral benefits of early dietary supplementation with CoEnzymeQ10 in a slowly progressing mouse model of Huntington's disease. Mol Cell Neurosci. (in press).
18. Kim, S Ho; Thomas, CA.; Andre, VM.; Cummings, DM.; Cepeda, C.; Levine, MS.; Ehrlich, ME. Forebrain striatal-specific expression of mutant huntingtin protein in vivo induces cell-autonomous age-dependent alterations in sensitivity to excitotoxicity and mitochondrial function. ASN Neuro. 2011; 3
19. Huntington's Disease Collaborative Research Group. A novel gene containing a trinucleotide repeat that is expanded and unstable on Huntington's disease chromosomes. Cell. 1993; 72:971–983. [PubMed: 8458085]
20. Ingham CA, Hood SH, Arbuthnott GW. Spine density on neostriatal neurones changes with 6-hydroxydopamine lesions and with age. Brain Res. 1989; 503:334–338. [PubMed: 2514009]
21. Ingham CA, Hood SH, Taggart P, Arbuthnott GW. Plasticity of synapses in the rat neostriatum after unilateral lesion of the nigrostriatal dopaminergic pathway. J. Neurosci. 1998; 18:4732–4743. [PubMed: 9614247]

22. Irwin SA, Idupulapati M, Gilbert ME, Harris JB, Chakravarti AB, Rogers EJ, Crisostomo RA, Larsen BP, Mehta A, Alcantara CJ, Patel B, Swain RA, Weiler IJ, Oostra BA, Greenough WT. Dendritic spine and dendritic field characteristics of layer V pyramidal neurons in the visual cortex of fragile-X knockout mice. Am. J. Med. Genet. 2002; 111:140–146. [PubMed: 12210340]
23. Johnson MA, Rajan V, Miller CE, Wightman RM. Dopamine release is severely compromised in the R6/2 mouse model of Huntington's disease. J. Neurochem. 2006; 97:737–746. [PubMed: 16573654]
24. Joshi PR, Wu NP, Andre VM, Cummings DM, Cepeda C, Joyce JA, Carroll JB, Leavitt BR, Hayden MR, Levine MS, Bamford NS. Age-dependent alterations of corticostriatal activity in the YAC128 mouse model of Huntington disease. J. Neurosci. 2009; 29:2414–2427. [PubMed: 19244517]
25. Kim SH, Thomas CA, Andre VM, Cummings DM, Cepeda C, Levine MS, Ehrlich ME. Forebrain striatal-specific expression of mutant huntingtin protein in vivo induces cell-autonomous age-dependent alterations in sensitivity to excitotoxicity and mitochondrial function. ASN Neuro. 2011; 3:e00060. [PubMed: 21542802]
26. Kish SJ, Shannak K, Hornykiewicz O. Elevated serotonin and reduced dopamine in subregionally divided Huntington's disease striatum. Ann. Neurol. 1987; 22:386–389. [PubMed: 2445259]
27. Klapstein GJ, Fisher RS, Zanjani H, Cepeda C, Jokel ES, Chesselet MF, Levine MS. Electrophysiological and morphological changes in striatal spiny neurons in R6/2 Huntington's disease transgenic mice. J. Neurophysiol. 2001; 86:2667–2677. [PubMed: 11731527]
28. Laforet GA, Sapp E, Chase K, McIntyre C, Boyce FM, Campbell M, Cadigan BA, Warzecki L, Tagle DA, Reddy PH, Cepeda C, Calvert CR, Jokel ES, Klapstein GJ, Ariano MA, Levine MS, DiFiglia M, Aronin N. Changes in cortical and striatal neurons predict behavioral and electrophysiological abnormalities in a transgenic murine model of Huntington's disease. J. Neurosci. 2001; 21:9112–9123. [PubMed: 11717344]
29. Lundin A, Dietrichs E, Haghighi S, Goller ML, Heiberg A, Loutfi G, Widner H, Wiktorin K, Wiklund L, Svenningsson A, Sonesson C, Waters N, Waters S, Tedroff J. Efficacy and safety of the dopaminergic stabilizer Pridopidine (ACR16) in patients with Huntington's disease. Clin. Neuropharmacol. 2010; 33:260–264. [PubMed: 20616707]
30. McGeer PL, McGeer EG. Neurotransmitters and their receptors in the basal ganglia. Adv. Neurol. 1993; 60:93–101. [PubMed: 8093584]
31. Melamed E, Hefti F, Bird E. Huntington chorea is not associated with hyperactivity of nigrostriatal dopaminergic neurons: Studies in postmortem tissues and in rats with kainic acid lesions. Neurology. 1982; 32:640–644. [PubMed: 6211637]
32. Menalled LB, Sison JD, Dragatsis I, Zeitlin S, Chesselet MF. Time course of early motor and neuropathological anomalies in a knock-in mouse model of Huntington's disease with 140 CAG repeats. J. Comp. Neurol. 2003; 465:11–26. [PubMed: 12926013]
33. Neely MD, Schmidt DE, Deutch AY. Cortical regulation of dopamine depletion-induced dendritic spine loss in striatal medium spiny neurons. Neuroscience. 2007; 149:457–464. [PubMed: 17888581]
34. Paulsen JS, Langbehn DR, Stout JC, Aylward E, Ross CA, Nance M, Guttman M, Johnson S, MacDonald M, Beglinger LJ, Duff K, Kayson E, Biglan K, Shoulson I, Oakes D, Hayden M. Detection of Huntington's disease decades before diagnosis: the Predict-HD study. J. Neurol. Neurosurg. Psychiatry. 2008; 79:874–880. [PubMed: 18096682]
35. Paxinos, G.; Franklin, KBJ. The Mouse Brain in Stereotaxic Coordinates. San Diego: Academic Press; 2001.
36. Phan J, Hickey MA, Zhang P, Chesselet MF, Reue K. Adipose tissue dysfunction tracks disease progression in two Huntington's disease mouse models. Hum Mol Genet. 2009; 18:1006–1016. [PubMed: 19124532]
37. Reisine TD, Fields JZ, Bird ED, Spokes E, Yamamura HI. Characterization of brain dopaminergic receptors in Huntington's disease. Commun. Psychopharmacol. 1978; 2:79–84. [PubMed: 149628]
38. Reisine TD, Fields JZ, Stern LZ, Johnson PC, Bird ED, Yamamura HI. Alterations in dopaminergic receptors in Huntington's disease. Life Sci. 1977; 21:1123–1128. [PubMed: 144230]

39. Restivo L, Ferrari F, Passino E, Sgobio C, Bock J, Oostra BA, Bagni C, Ammassari-Teule M. Enriched environment promotes behavioral and morphological recovery in a mouse model for the fragile X syndrome. Proc. Natl. Acad. Sci. USA. 2005; 102:11557–11562. [PubMed: 16076950]
40. Rosas HD, Hevelone ND, Zaleta AK, Greve DN, Salat DH, Fischl B. Regional cortical thinning in preclinical Huntington disease and its relationship to cognition. Neurology. 2005; 65:745–747. [PubMed: 16157910]
41. Rosas HD, Lee SY, Bender AC, Zaleta AK, Vangel M, Yu P, Fischl B, Pappu V, Onorato C, Cha JH, Salat DH, Hersch SM. Altered white matter microstructure in the corpus callosum in Huntington's disease: implications for cortical "disconnection". Neuroimage. 2010; 49:2995–3004. [PubMed: 19850138]
42. Rosas HD, Liu AK, Hersch S, Glessner M, Ferrante RJ, Salat DH, van der Kouwe A, Jenkins BG, Dale AM, Fischl B. Regional and progressive thinning of the cortical ribbon in Huntington's disease. Neurology. 2002; 58:695–701. [PubMed: 11889230]
43. Rosas HD, Tuch DS, Hevelone ND, Zaleta AK, Vangel M, Hersch SM, Salat DH. Diffusion tensor imaging in presymptomatic and early Huntington's disease: Selective white matter pathology and its relationship to clinical measures. Mov. Disord. 2006; 21:1317–1325. [PubMed: 16755582]
44. Slow EJ, van Raamsdonk J, Rogers D, Coleman SH, Graham RK, Deng Y, Oh R, Bissada N, Hossain SM, Yang YZ, Li XJ, Simpson EM, Gutekunst CA, Leavitt BR, Hayden MR. Selective striatal neuronal loss in a YAC128 mouse model of Huntington disease. Hum Mol Genet. 2003; 12:1555–1567. [PubMed: 12812983]
45. Smith MA, Brandt J, Shadmehr R. Motor disorder in Huntington's disease begins as a dysfunction in error feedback control. Nature. 2000; 403:544–549. [PubMed: 10676962]
46. Stephens B, Mueller AJ, Shering AF, Hood SH, Taggart P, Arbuthnott GW, Bell JE, Kilford L, Kingsbury AE, Daniel SE, Ingham CA. Evidence of a breakdown of corticostriatal connections in Parkinson's disease. Neuroscience. 2005; 132:741–754. [PubMed: 15837135]
47. Tabrizi SJ, Langbehn DR, Leavitt BR, Roos RA, Durr A, Craufurd D, Kennard C, Hicks SL, Fox NC, Scahill RI, Borowsky B, Tobin AJ, Rosas HD, Johnson H, Reilmann R, Landwehrmeyer B, Stout JC. Biological and clinical manifestations of Huntington's disease in the longitudinal TRACK-HD study: cross-sectional analysis of baseline data. Lancet Neurol. 2009; 8:791–801. [PubMed: 19646924]
48. Tabrizi SJ, Scahill RI, Durr A, Roos RA, Leavitt BR, Jones R, Landwehrmeyer GB, Fox NC, Johnson H, Hicks SL, Kennard C, Craufurd D, Frost C, Langbehn DR, Reilmann R, Stout JC. Biological and clinical changes in premanifest and early stage Huntington's disease in the TRACK-HD study: the 12-month longitudinal analysis. Lancet Neurol. 2011; 10:31–42. [PubMed: 21130037]
49. Tang TS, Chen X, Liu J, Bezprozvanny I. Dopaminergic signaling and striatal neurodegeneration in Huntington's disease. J. Neurosci. 2007; 27:7899–7910. [PubMed: 17652581]
50. Thomas EA, Coppola G, Tang B, Kuhn A, Kim S, Geschwind DH, Brown TB, Luthi-Carter R, Ehrlich ME. In vivo cell-autonomous transcriptional abnormalities revealed in mice expressing mutant huntingtin in striatal but not cortical neurons. Hum. Mol. Genet. 2011; 20:1049–1060. [PubMed: 21177255]
51. van Oostrom JC, Maguire RP, Verschuuren-Bemelmans CC, Veenma-van der Duin L, Pruim J, Roos RA, Leenders KL. Striatal dopamine D2 receptors, metabolism, and volume in preclinical Huntington disease. Neurology. 2005; 65:941–943. [PubMed: 16186542]

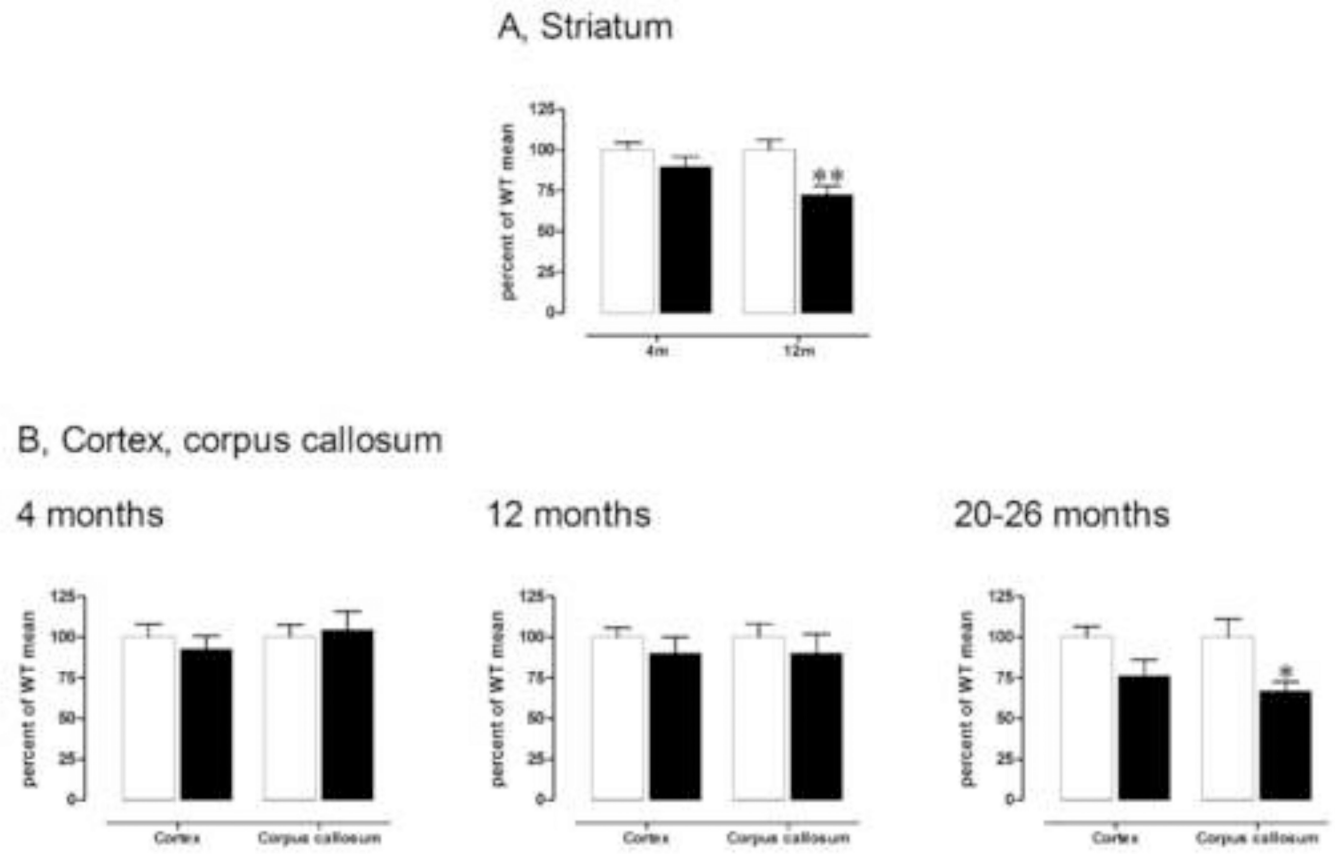

Fig. 1.

A) Male homozygous KI mice exhibit a striatal volume loss, with a significant 27% reduction, by 12 months of age. **p<0.01 compared to WT, same timepoint. Data are mean ± sem (4 months, n=4–5; 12 months, n=3–4). B) Male homozygous KI mice show significant volume reduction in the corpus callosum by 20–26 months of age (right). *p<0.05 compared to WT, same timepoint. Data are mean ± sem (4 months, left, n=4–5; 12 months, middle, n=3–4; 20–26, right, months; n=4–7). Volumes of striatum are measured at from bregma +1.94 through −0.46 [35] and cortical and corpus callosum volumes are measured from these same sections. See text for details on statistical analyses.

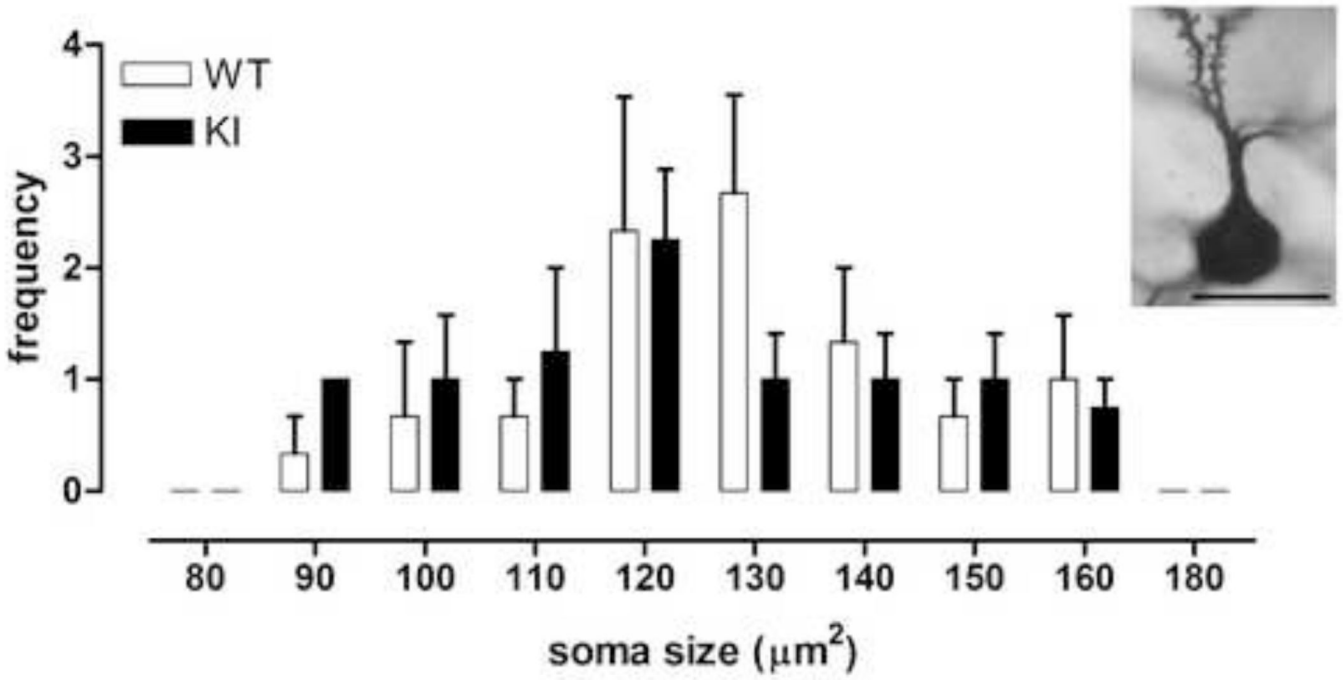

Fig. 2.

Frequency distribution of soma sizes in Golgi-stained MSSNs from 20–26 month old male WT (n=3) and male homozygous KI mice (n=4). Medium sized spiny neurons were drawn using a camera lucida and features measured from these drawings. Insert: Photomicrograph of part of a representative golgi-stained MSSN observed through a CHS Olympus Hi Tech Instruments, Inc. microscope. Scalebar: 20 μm.

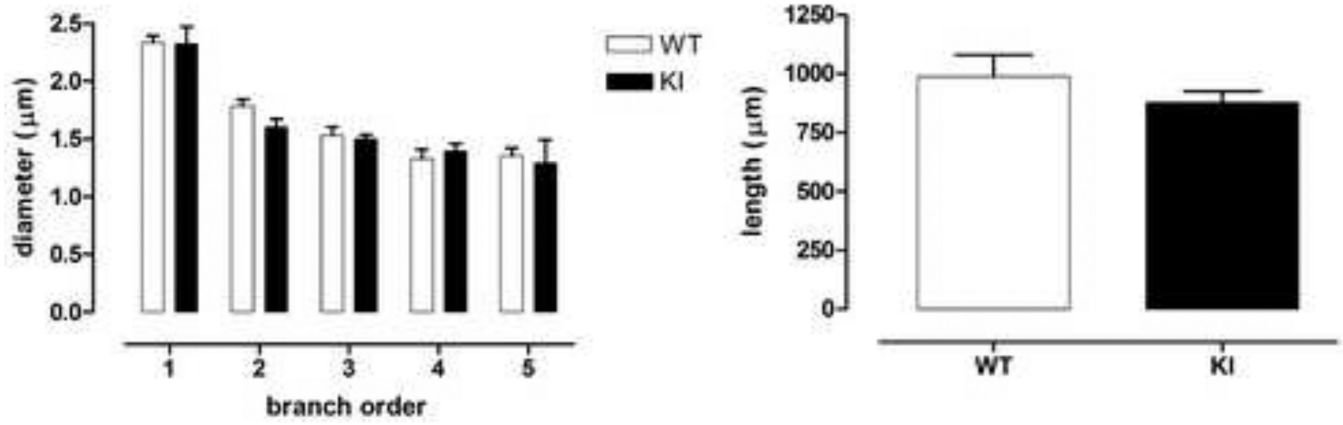

Fig. 3.

No differences were observed in the branch diameter (left) or total branch length (right) between male WT and male homozygous KI mice. However, KI mice showed a slight trend towards reduced total branch length. Data (mean ± sem; n=3–4) were analyzed with ANOVA followed by Fisher's LSD post hoc tests (dendritic diameter) or Student's t test (branch length).

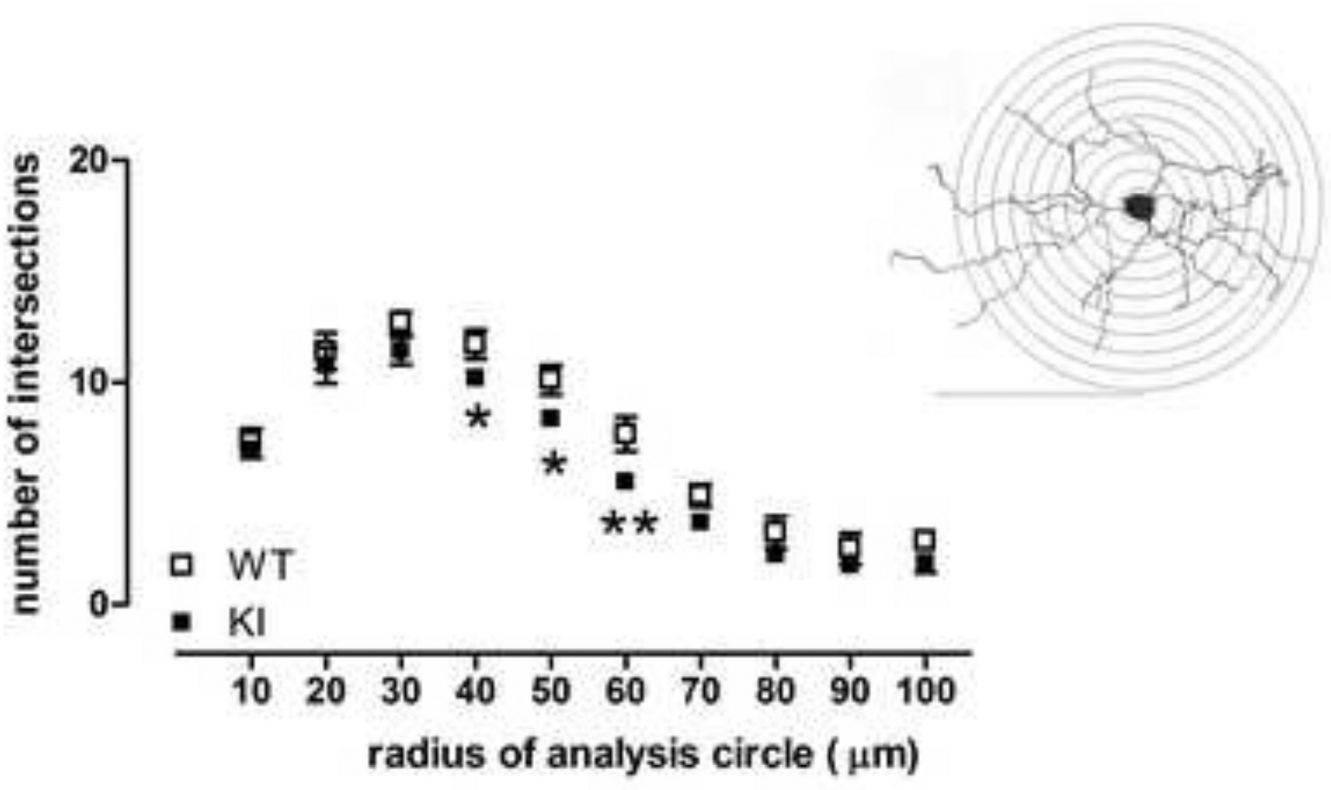

Fig. 4.

Sholl analysis of medium sized spiny neurons in 20–26 month-old male WT and male homozygous KI CAG140 mice revealed that KI mice show fewer dendritic intersections, indicating loss of dendritic field, when compared to WT mice. *p<0.05, **p<0.01 compared to WT. Inset: Example of Sholl concentric circles, placed over a Golgi-stained MSSN drawn using camera lucida technique. Bar = 100 μm. Data (mean ± sem; n=3–4) were analyzed with ANOVA followed by Fisher's LSD post hoc tests.

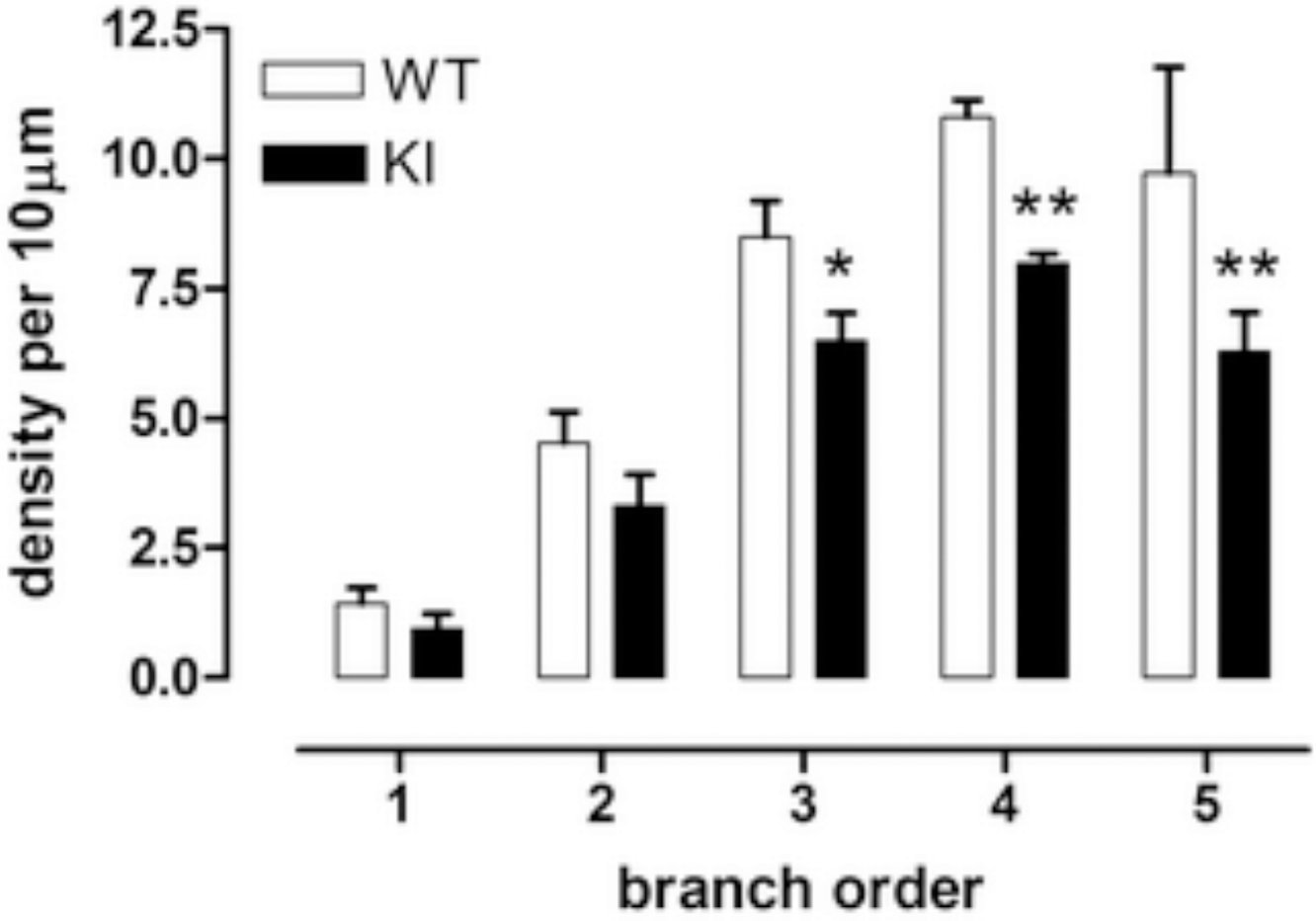

Fig. 5.

Spine density in Golgi-stained medium sized spiny striatal neurons was significantly reduced in male homozygous KI mice at branch orders 3, 4, and 5. *p<0.05, **p<0.01 compared to male WT, same branch order. Data (mean ± sem, n=3–4) were analyzed using ANOVA followed by Fisher's LSD post hoc tests.

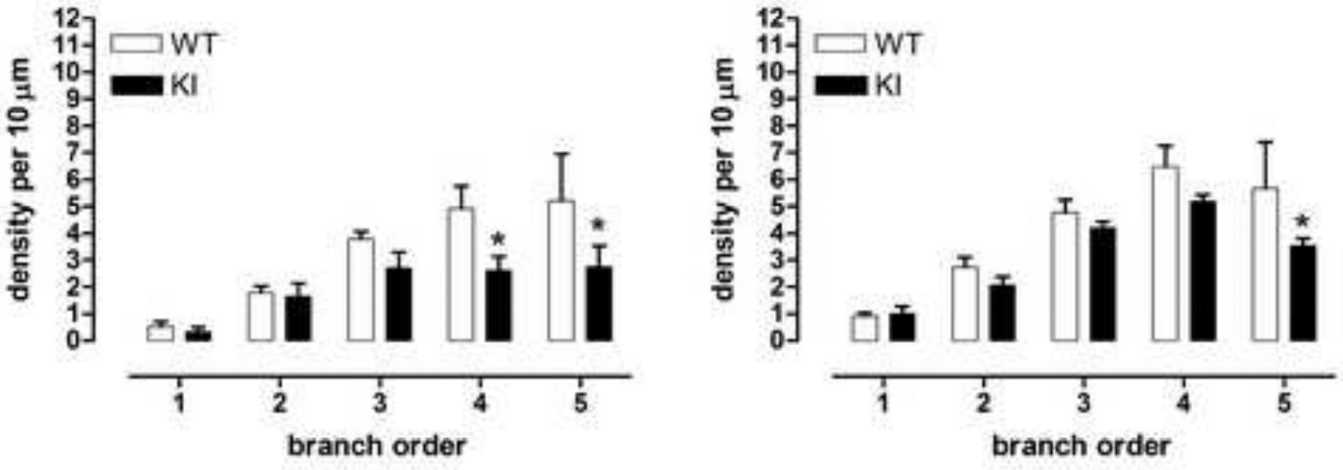

Fig. 6.

Male homozygous KI mice exhibited a loss of both immature and mature spines, with greater loss of immature spines, *p<0.05. Data (mean ± sem, n=3–4) were analyzed using ANOVA followed by Fisher's LSD post hoc tests.

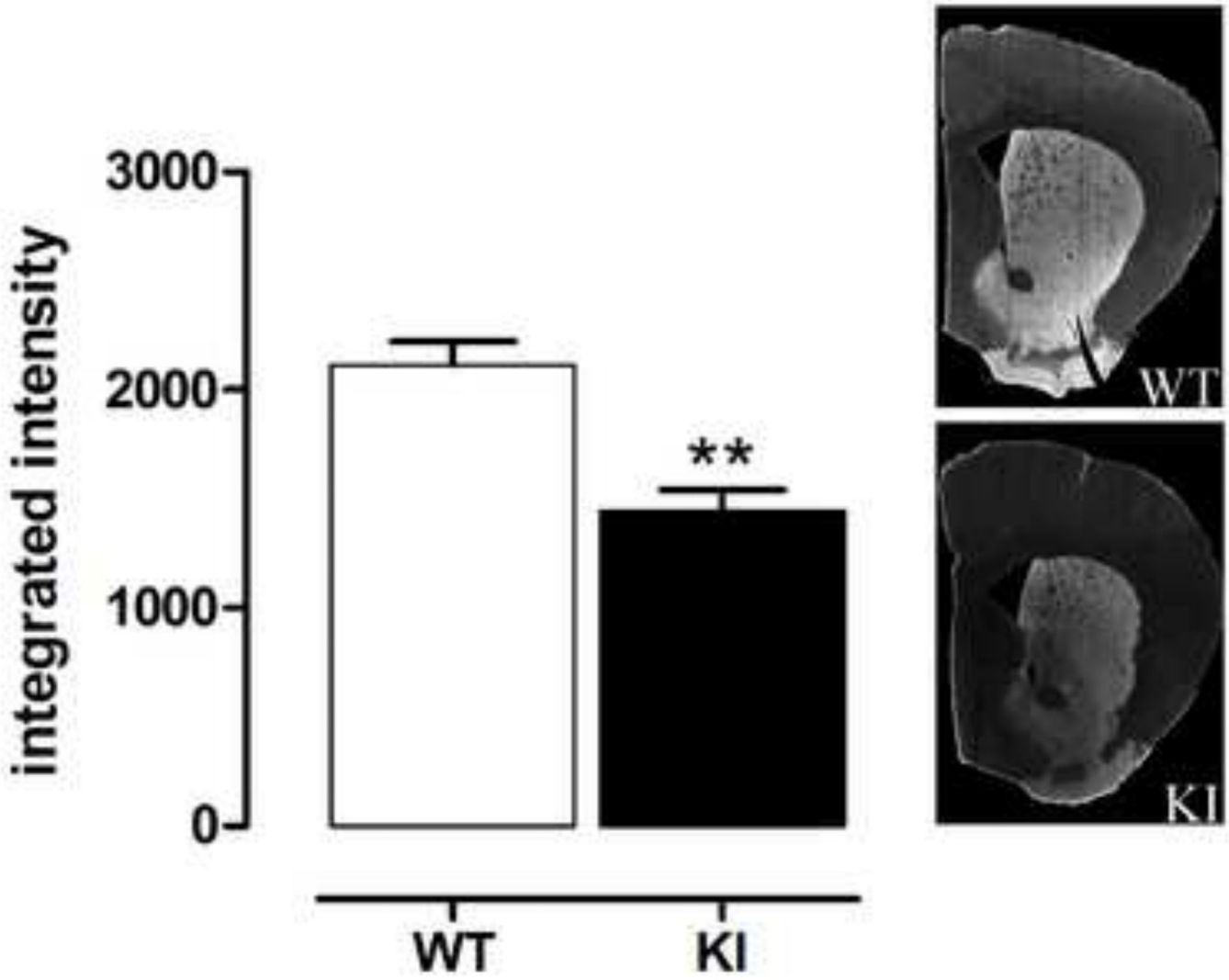

Fig. 7.

Male homozygous KI mice show significant loss of striatal TH immunostaining, by 20–26 months of age. Sections were stained for TH, using fluorescence and the fluorescence intensity quantified using a microarray scanner. KI mice showed 32% loss in TH intensity (mean ± sem, n=5–6). **p<0.01 compared to WT, Student's t test. Right: representative photomicrographs of immunostaining.